



# Effect of high-intensity ultrasonic treatment on modification of primary Mg<sub>2</sub>Si in the hypereutectic Mg–Si alloys



M.E. Moussa<sup>a,\*</sup>, M.A. Waly<sup>a</sup>, A.M. El-Sheikh<sup>b</sup>

<sup>a</sup> Department of Manufacturing Technology, Laboratory of Foundry, Central Metallurgical Research and Development Institute (CMRDI), P.O. 87, Halwan, Egypt

<sup>b</sup> Department of Mining, Petroleum and Metallurgical Engineering, Faculty of Engineering, Cairo University, P.O. 12613, Giza, Egypt

## ARTICLE INFO

### Article history:

Received 19 May 2013

Received in revised form 17 June 2013

Accepted 29 June 2013

Available online 8 July 2013

### Keywords:

Metals and alloys

Microstructure

Thermal analysis

Metallography

## ABSTRACT

The effect of high intensity ultrasonic treatment (HIUST) on modification of primary Mg<sub>2</sub>Si in the hypereutectic Mg–5 wt.%Si alloy have been studied. Various resulted microstructures were produced in this alloy by employing ultrasonic vibrations during solidification process at different pouring temperatures and for different application times. The results showed clearly that in the absence of HIUST, the dendrites of primary Mg<sub>2</sub>Si were coarser and non-uniform in size. Upon HIUST of the alloy during solidification process, nearly uniform and polyhedral shape of primary Mg<sub>2</sub>Si with a network of Mg phase segregated along the grain boundaries were obtained. Interestingly, the average size of primary Mg<sub>2</sub>Si decreased significantly with increasing the pouring temperature and the vibration time of HIUST reached a minimum at 800 °C and 90 s. After that the average size of primary Mg<sub>2</sub>Si increased slightly with further increasing the pouring temperature and the ultrasonic vibration time. Modification mechanism resulting in the development of microstructure is also investigated.

© 2013 Elsevier B.V. All rights reserved.

## 1. Introduction

Magnesium alloys are widely applied in the fields which are strongly driven towards weight-reduction, such as automotive, aeronautic and astronautic industries [1–4]. Meanwhile, improving the elevated temperature properties of magnesium alloys has become a critical issue for the further application [5–7]. In recent years, the fascinating properties and promising application of hypereutectic Mg–Si alloys have attracted particular interest due to the formation of thermally stable Mg<sub>2</sub>Si phase [7–9]. It is known that the intermetallic compound of Mg<sub>2</sub>Si exhibits an excellent combination of superior properties, such as high melting temperature (1085 °C), low density ( $1.99 \times 10^3 \text{ kg m}^{-3}$ ), high hardness ( $4.5 \times 10^9 \text{ N m}^{-2}$ ), low thermal expansion coefficient ( $7.5 \times 10^{-6} \text{ K}^{-1}$ ) and reasonably high elastic modulus (120 GPa). Furthermore, the Mg<sub>2</sub>Si phase is exceptionally stable and therefore could effectively impede grain boundary sliding at elevated temperatures [8–13]. However, the hypereutectic Mg–Si alloys prepared by ordinary ingot metallurgy process showed very low ductility and strength due to the large primary Mg<sub>2</sub>Si particle size and the brittle eutectic phase [12,13].

Various researches are aimed at improving the mechanical properties of Mg<sub>2</sub>Si reinforced Mg-alloys through processes, such as hot extrusion [14], rapid solidification [15] and mechanical

alloying [16]. However, compared with the above-mentioned techniques, modification treatment is a more cost-effective processing technique and available for generally commercial application. Much work has been focused on the modification effects of Ca [4], P [6], Sr–Sb [7,8], Y [12], Sr [17], Sb [18,19], Ba [20], KBF<sub>4</sub> [21,22], Bi [23], and Y<sub>2</sub>O<sub>3</sub> [24] on the primary and eutectic Mg<sub>2</sub>Si in magnesium alloys. However, certain internal defects could be existed. For example, although KBF<sub>4</sub> has a good effect on the modification of Mg<sub>2</sub>Si phase in Mg–5Si alloys, a large quantity of smoke and sputter is produced, which is harmful to the surrounding environment [21,22]. Y [12], Ba [20] and Bi [23] can modify and refine the primary Mg<sub>2</sub>Si, but the Mg<sub>2</sub>Si phase becomes coarse again when the adding amount exceeds a certain limit. Therefore, an alternative method for the development of hypereutectic Mg–Si alloys with modification of Mg<sub>2</sub>Si phase and high mechanical properties is desired.

HIUST is a simple and effective physical method for solidification control. Investigations carried out between 1960 and 1990 [25,26], mainly in the former Soviet Union countries, clearly demonstrated its grain-refinement effects on magnesium alloys and significantly improved mechanical properties. The renewed interest in magnesium materials in recent years has resulted in increased attention in the grain-refinement potential of HIUST for magnesium alloys [27–37], particularly for Mg–Al based alloys. However, seldom investigation has been carried out with regard to the modification effect of HIUST on morphology of primary Mg<sub>2</sub>Si in hypereutectic Mg–Si alloys.

\* Corresponding author. Tel./fax: +20 2 25010095.

E-mail address: [eissa83@yahoo.com](mailto:eissa83@yahoo.com) (M.E. Moussa).

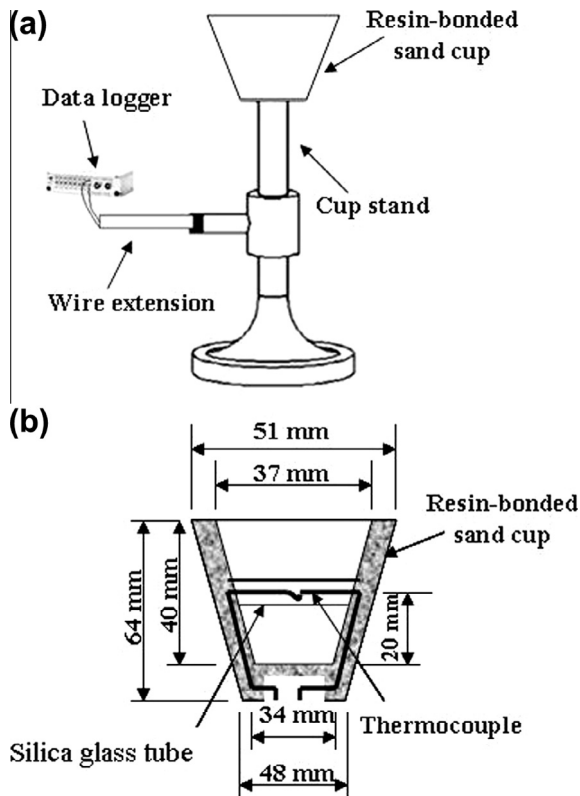


Fig. 1. Schematic of (a) experimental setup for thermal analysis and (b) resin-bonded sand cup with type K thermocouple.

The main purpose of the present work is to study the modification effect of HIUST on morphology of primary  $Mg_2Si$  in the hypereutectic Mg–5 wt.%Si alloy. The experiments that involved vibrating the molten alloy during solidification process are performed under the application of HIUST at different pouring temperatures and vibration times.

Table 1

The chemical composition of prepared Mg–5 wt.%Si alloy (wt.%).

Si	Fe	Cu	Ni	Mg
5	0.022	0.015	0.0034	Bal.

## 2. Experimental procedures

### 2.1. Materials and processing

Commercial pure Mg (99.8 wt.% purity) and Si (99.9 wt.% purity) were used as starting materials. Charges of about 15 kg with the nominal composition of hypereutectic Mg–5 wt.%Si alloy were prepared as the base material in the present study. The charge was melted in a graphite crucible by a 200 kW medium frequency induction furnace under the mixed gas protection consists of tetrafluoroethane ( $CF_3CH_2F$ , HFC-134a, 1 vol.%) and carbon dioxide ( $CO_2$ , Bal.). Firstly commercial Mg ingots were melted to above 650 °C, and then silicon was added into Mg melt. After that the melt were heated to above 800 °C and kept about 30 min to ensure Mg and Si fully reacted and formed  $Mg_2Si$ . Finally the melt was poured into a cast iron mold.

The solidification characteristic of the prepared alloy was confirmed using thermal analysis in order to designate experimental conditions. The thermal analysis test sample was obtained by pouring the quantity of the melt at 800 °C into standard Qjuk-Cup resin-bonded sand cup with dimensions described in Fig. 1. A high sensitivity type K thermocouple (chromel–alumel) located horizontally at the center of the cup, facilitated the capturing of the temperature during solidification. The thermocouple within the mold was protected using silica glass tube. The data for thermal analysis were collected using a data logger and transferred to a personal computer for analysis. Thermal analysis trial was repeated three times to ensure reproducibility of the results. From the thermal analysis data, the cooling curve with its first derivative curve was plotted as shown in Fig. 2. The primary  $Mg_2Si$  began to precipitate from the prepared alloy melt at 767 °C and the eutectic reaction occurred at about 637.1 °C. The chemical compositions of the prepared alloy were measured with inductive coupled plasma optical emission spectroscopy (ICP-OES) (model Optima 2000, Germany), as shown in Table 1.

The ultrasonic treated samples were prepared as following. The hypereutectic Mg–5 wt.%Si alloy of about 1 kg was melted at 800 °C in a mild steel crucible using an electric resistance furnace under the mixed gas protection consists of tetrafluoroethane ( $CF_3CH_2F$ , HFC-134a, 1 vol.%) and carbon dioxide ( $CO_2$ , Bal.). The melt was manually stirred for 2 min using a stainless steel rod, and then was held for additional 10 min in order to get full homogenization. After that the slag was removed, and then the melt was poured into a cylindrical resin-bonded sand mold with dimensions of outer diameter ( $\varnothing$  100 mm), inner diameter ( $\varnothing$  42 mm) and length (250 mm) which mounted on the ultrasonic sonotrode of diameter ( $\varnothing$  40 mm) as shown in Fig. 3. The reason for using a cylindrical resin-bonded sand mold is to reduce the cooling rate effect on the resulted microstructures of the prepared

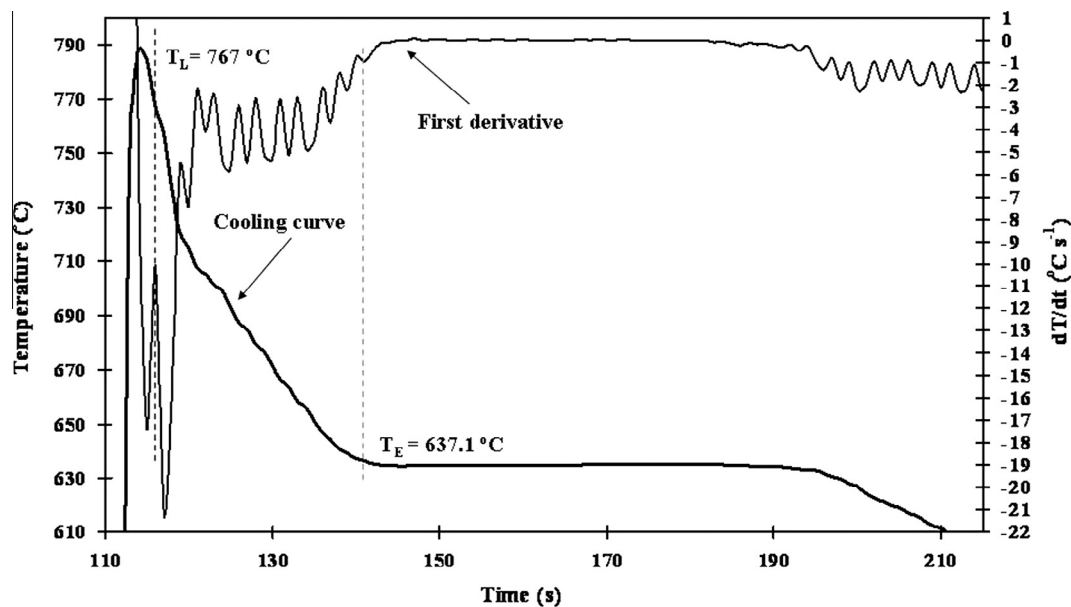


Fig. 2. The cooling curve with its first derivative curve of the investigated hypereutectic Mg–5 wt.%Si alloy.

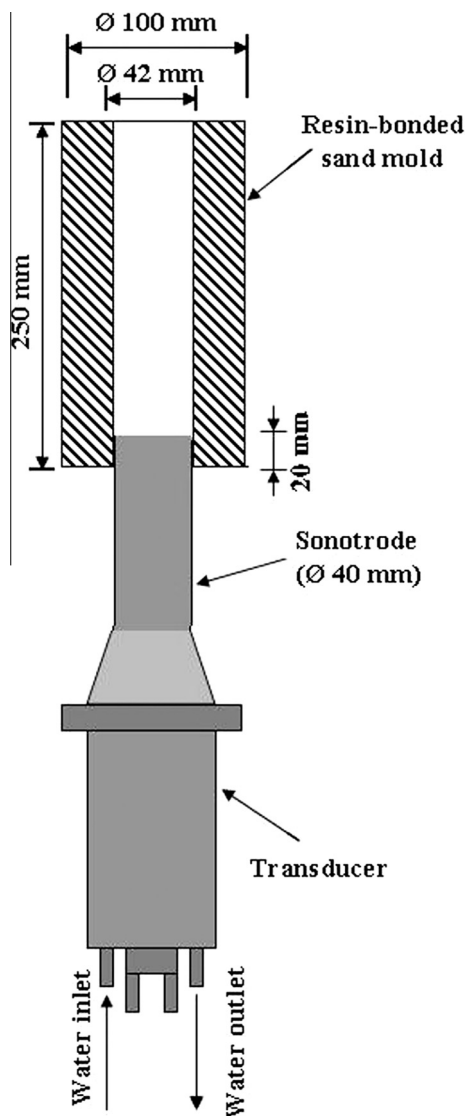


Fig. 3. Schematic of the experimental setup used in this study.

samples. Therefore, the difference in the morphology and size of primary  $Mg_2Si$  in the microstructures of investigated samples were obtained mainly as a result of the difference in the application of HIUST conditions.

Two types of experiments were carried out, namely the first group and the second group. In the first group, HIUST which was generated by using ultrasonic generator (model TS6MD1, Russia) and magnetostrictive transducer (model PMS-15-22, Russia) with the maximum output power of 5 KW and the fixed frequency of 21.4 kHz was applied right before the melt was poured into cylindrical resin-bonded sand mold. The HIUST effect was studied in this group at different designated pouring temperatures (770, 780, 790, 800, 810 °C) for 90 s above the liquidus temperature of the investigated alloy of 767 °C (Fig. 2). At the end of planned HIUST application time, the ultrasonic source was switched off and the melt was left to room temperature. Pouring temperatures were controlled within an accuracy of  $\pm 2$  °C. The ultrasonic waves emitted from the transducer and passed through the acoustic sonotrode were propagated directly into the melt during solidification. The poured melt became a part of acoustic sonotrode, so the action of ultrasonic energy on the melt was raised remarkably. For comparison, a sample without the application of HIUST was prepared at pouring temperature of 800 °C. In the second group, the application of HIUST was carried out for different vibration times 10, 50, 90, 130 s at optimum pouring temperature based on the results of the first group.

## 2.2. Materials characterization

All metallographic specimens were cut from the bottom of castings at the same position of 10 mm above the sonotrode contact level of cylindrical samples. The samples were prepared according to usual procedures developed for magnesium alloys [38] and etched by solution with 10 ml nitric acid, 30 ml acetic acid, 40 ml

water, and 120 ml ethanol for 2–3 min. The microstructures of the specimens were analyzed by optical microscope (OM) (model OPTIKA M-790, Italy). In the present study, the average length of primary  $Mg_2Si$  was measured as the size of  $Mg_2Si$ . Six OM micrographs were taken for each sample from the observed area at a low magnification of 100 $\times$ . The average size of the primary  $Mg_2Si$  was measured by ImageJ1.44 software. All  $Mg_2Si$  existed in one picture taken from the observed area were measured.

Energy dispersion spectrum (EDS) (model INCA PENTAFET X3, England) affiliated to the scanning electron microscope (SEM) (model JSM-5410, Japan) was performed to reveal the concentration of alloying elements in selected areas of the microstructure. Phase constituents of samples were analyzed by X-ray diffraction (XRD) (model X'PERT PRO, The Netherlands) using Cu K $\alpha$  radiation in step scan of  $2\theta$  from 20° to 80° with an increment of 0.02° and a scanning speed of 4°/min.

## 3. Results

### 3.1. The first group

According to the Mg–Si binary phase diagram [39], Mg–5 wt.%Si alloy is a typical hypereutectic alloy. As-cast microstructures of Mg–5 wt.%Si alloy processed without and with HIUST at different pouring temperatures for 90 s are shown in Fig. 4a–f. The microstructures of hypereutectic base alloy reveal the presence of primary  $Mg_2Si$ , Mg halos and eutectic Mg– $Mg_2Si$ . Moreover, all the primary  $Mg_2Si$  are surrounded by Mg halos, and then by eutectic structure [8]. Without HIUST, the primary  $Mg_2Si$  shows a coarse dendritic morphology with the average size of about 200  $\mu m$ , as shown in Fig. 4a.

With the application of HIUST for 90 s at pouring temperature of 770 °C, most of primary  $Mg_2Si$  phases are still dendrite, but their average size are reduced significantly to about 80  $\mu m$ , as shown in Fig. 4b. As the pouring temperature increases from 780 to 800 °C, most of primary  $Mg_2Si$  phases become polyhedral shape and their average size are reduced from about 43 to 33  $\mu m$  respectively, as shown in Fig. 4c–e. When the pouring temperature is further increased to 810 °C, the average size of primary  $Mg_2Si$  increases slightly again to about 43  $\mu m$ , as shown in Fig. 4f. Therefore, under the application of HIUST at different pouring temperatures for 90 s, the average size of primary  $Mg_2Si$  decreases significantly with increasing pouring temperature, reaches a minimum at 800 °C, and then increases slightly with further increasing pouring temperature as compared without the application of HIUST, as shown in Fig. 5.

To ascertain phase constituents, composition and structure of the based hypereutectic Mg–5 wt.%Si alloys, XRD and EDS were conducted for both conditions without and with HIUST at pouring temperature of 800 °C for 90 s respectively. XRD results reveal that the constituents of the obtained microstructures for both conditions without and with HIUST are only  $Mg_2Si$  and Mg phases, as shown in Fig. 6. Therefore, no change of the phase constituents obtained due to HIUST.

The SEM image, EDS line scan and EDS elemental mapping of Si and Mg for the based hypereutectic Mg–5 wt.%Si alloy without and with HIUST at pouring temperature of 800 °C for 90 s are shown in Figs. 7 and 8, respectively. It can be seen that the coarse primary  $Mg_2Si$  is formed by the preferred growth that occurs at the tips of branches in the alloy without HIUST (Fig. 7a), resulting in complex regular, sharp-angled and dendritic morphologies with a non-uniform distribution of Mg in the interdendritic regions (Fig. 7b–d). With the HIUST, the morphology of primary  $Mg_2Si$  changes from coarse dendritic structure to fine polyhedral shape (Fig. 8a) with a network of Mg segregated along the grain boundaries (Fig. 8b–d).

### 3.2. The second group

The second group was carried out at optimum pouring temperature of 800 °C based on the results of the first group for different ultrasonic vibration times of 10, 50, 90 and 130 s. With the application of HIUST for 10 s, the morphologies of primary  $Mg_2Si$  are

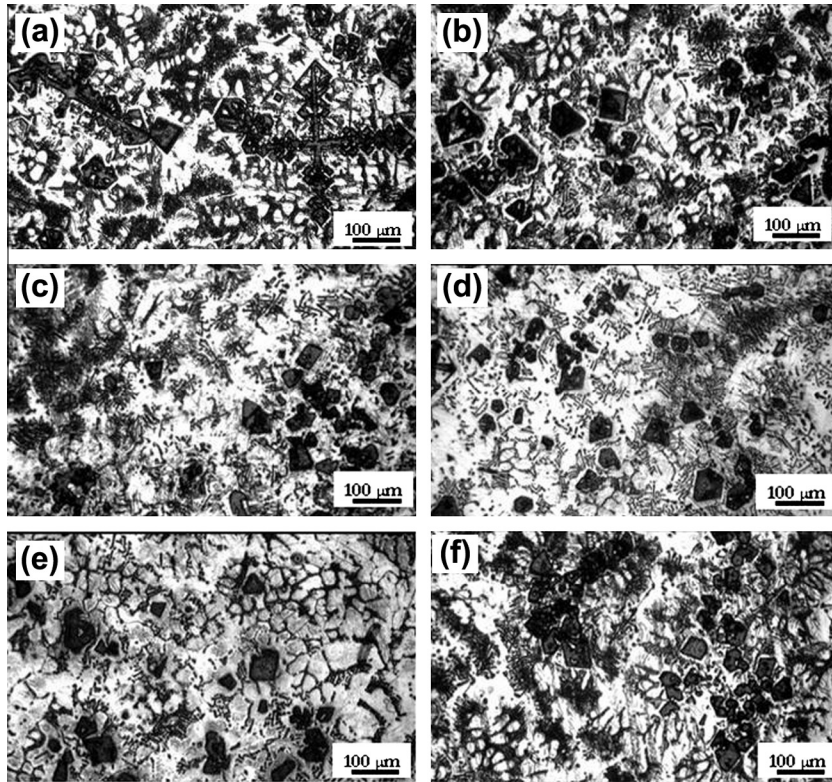


Fig. 4. OM micrographs of the investigated hypereutectic Mg–5 wt.%Si alloy processed (a) without HIUST at pouring temperature of 800 °C and with HIUST for 90 s at different pouring temperatures of (b) 770 °C, (c) 780 °C, (d) 790 °C, (e) 800 °C and (f) 810 °C.

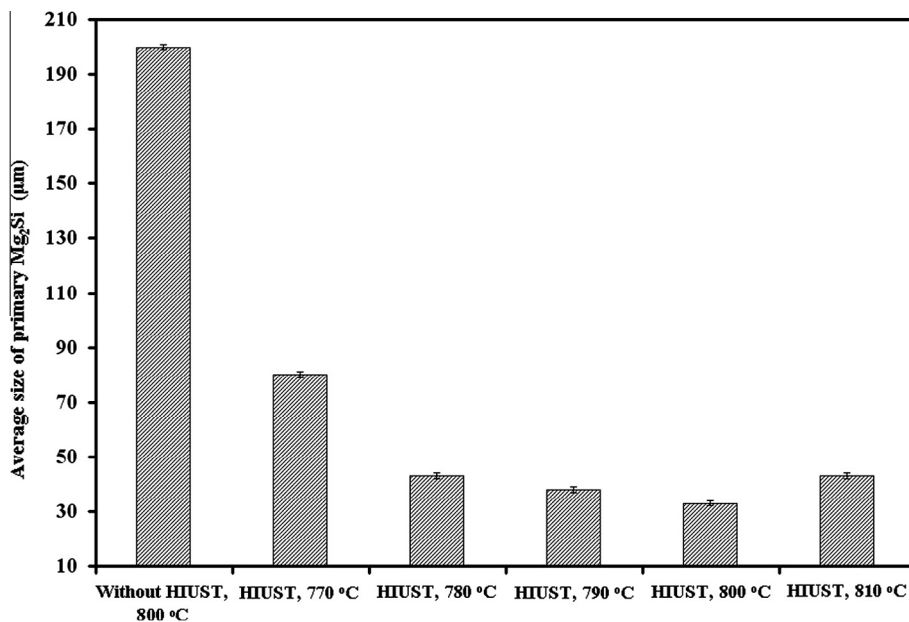


Fig. 5. Variation of average size of primary Mg<sub>2</sub>Si of the investigated hypereutectic Mg–5 wt.%Si alloys without and with HIUST at different pouring temperatures for 90 s.

mixture of dendritic and octahedron structure and their average size are about 58 μm, as shown in Fig. 9a. As vibration time increases from 50 to 90 s, most of primary Mg<sub>2</sub>Si phases become polyhedral shape and their average size are slightly reduced from about 35 (Fig. 9b) to 33 μm (Fig. 4e), respectively. When the vibration time is further increased to 130 s, the average size of primary Mg<sub>2</sub>Si increases slightly again to about 45 μm, as shown in Fig. 9c. The variation of average size of primary Mg<sub>2</sub>Si with the ultrasonic

vibration times is shown in Fig. 10 for HIUST done at optimum pouring temperature of 800 °C.

#### 4. Discussion

Under the present experimental conditions, the effect of the cooling rate on the modification of primary Mg<sub>2</sub>Si in hypereutectic Mg–5 wt.%Si could be negligible. Therefore, the difference in the

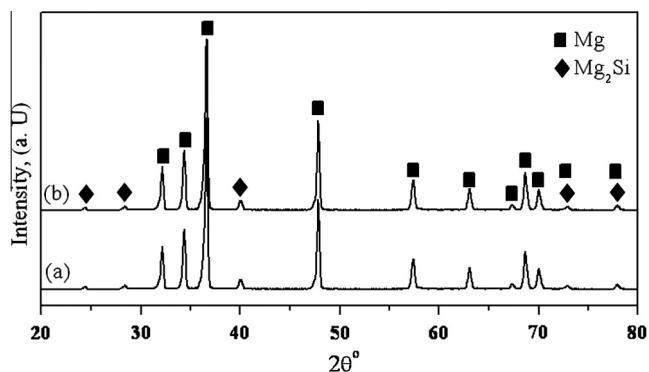


**Fig. 6.** XRD patterns of the investigated hypereutectic Mg–5 wt.%Si alloys (a) without and (b) with HIUST at optimum pouring temperature of 800 °C for 90 s.

morphology and size of primary  $Mg_2Si$  were resulted almost exclusively from the difference in the application of HIUST conditions. Usually, the microstructure of materials depends on the nucleation process and growth conditions [31]. For the  $Mg_2Si$ , its structure belongs to face centered cube (FCC) and its dendrite arm should grow along the preferential [100] crystallographic directions [22]. As a result, the morphologies of primary  $Mg_2Si$  in the sample without HIUST are mainly characterized by dendrites with complex morphologies, as shown in Figs. 4a and 7a.

The refinement and modification of primary  $Mg_2Si$  can be mainly attributed to HIUST during the solidification process. This can be explained as conjugation of two mechanisms: cavitation-

enhanced heterogeneous nucleation and cavitation-induced dendrite fragmentation. During the first stage of solidification between pouring temperatures and the liquidus temperature of the investigated alloy, HIUST can only be attributed to cavitation-enhanced heterogeneous nucleation. This because dendrite fragmentation will not be possible at those temperatures since solidification has not started yet. The cavitation-enhanced heterogeneous nucleation is further explained by three different mechanisms. The first is based on the pressure pulse-melting point ( $T_m$ ) mechanism [27,34,40,41], where the pressure pulse arising from the collapse of bubbles alters  $T_m$  according to the Clausius–Clapeyron equation as  $dT_m/dP = T_m(V_L - V_S)/\Delta H$ , where  $T_m$  is the freezing point in K,  $P$  is the pressure in MPa,  $V_L$  and  $V_S$  are the specific volume of the liquid and the solid phase in  $cm^3/g$ , respectively, and  $\Delta H$  is the latent heat of freezing in J. An increase in  $T_m$  is equivalent to increasing the undercooling so that an enhanced nucleation event is expected. The second is based on cavitation-enhanced wetting [26], which assumes that cavities and cracks on the substrate surfaces and insoluble non-metallic inclusions that either pre-exist in the melt or form on cooling during solidification, can be wetted by the melt under the pressure pulse from the collapse of the bubbles. Consequently, this enables these substrates to act as effective nucleation sites. The third mechanism [30,40,42] assumes that rapid adiabatic expansion of gas inside the bubbles created during cavitation undercools the liquid at the bubble–liquid interfaces resulting in nucleation on the bubble surfaces. Collapsing of these bubbles will distribute the nuclei into the surrounding liquid producing a significant number of nuclei in the liquid.

Below the liquidus temperature investigated, corresponding to the formation of the first solid metal, the cavitation-induced

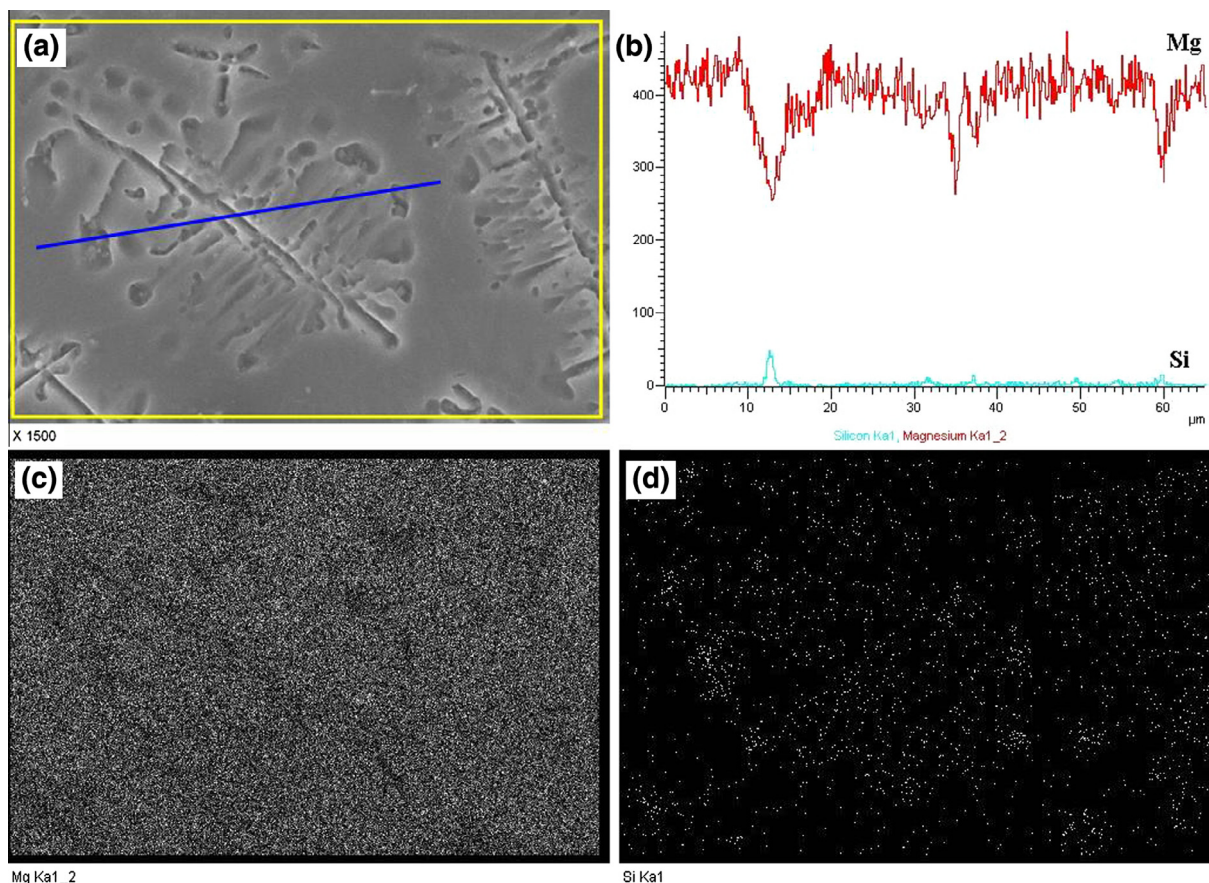


**Fig. 7.** (a) SEM micrograph, (b) EDS line scans of Mg and Si, (c) EDS elemental mapping of Mg and (d) EDS elemental mapping of Si for the investigated hypereutectic Mg–5 wt.%Si alloy without HIUST at pouring temperature of 800 °C.

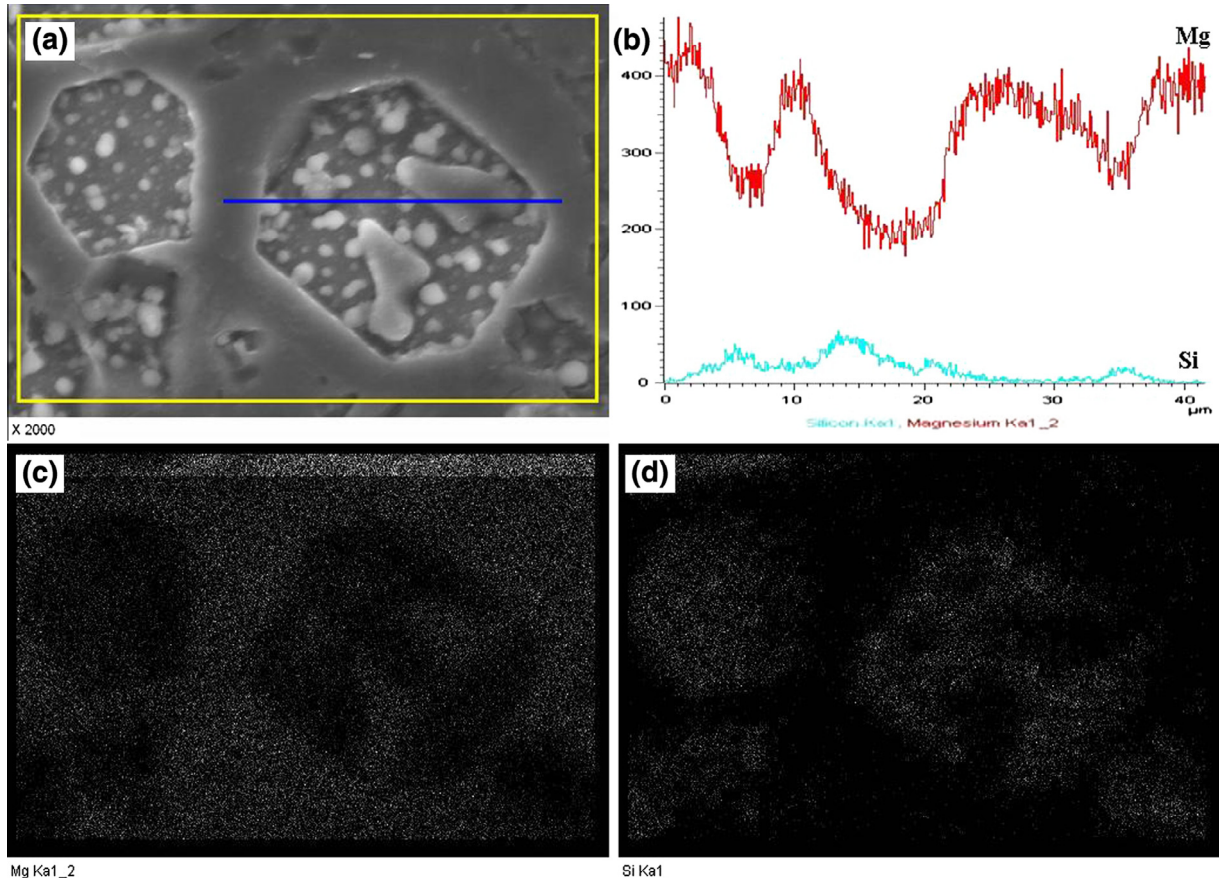


**Fig. 8.** (a) SEM micrograph, (b) EDS line scans of Mg and Si, (c) EDS elemental mapping of Mg and (d) EDS elemental mapping of Si for the investigated hypereutectic Mg–5 wt.%Si alloy with HIUST at pouring temperature of 800 °C for 90 s.

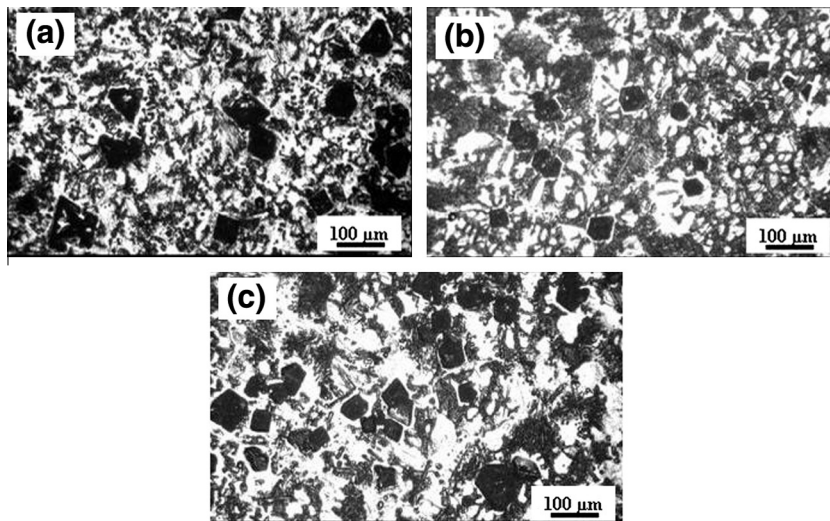


**Fig. 9.** OM micrographs of the investigated hypereutectic Mg–5 wt.%Si alloys processed with HIUST at optimum pouring temperature of 800 °C for (a) 10 s, (b) 50 s and (c) 130 s.

dendrite fragmentation is more effective and dominant. This mechanism assumes that the shock waves generated from the collapse of bubbles lead to fragmentation of dendrites [29,34,41,43], which are redistributed through acoustic streaming, thereby increasing the number of crystals. The coexistence of these two mechanisms seems to promote a high density of nuclei in the melt, thus leading to the development of a large number of fine primary  $Mg_2Si$  crys-

tals which exhibit an octahedral morphologies [8] with a variety of polygonal outlines in the two-dimensional view, such as triangle, square, trapezoid and hexagon because of the random cutting angles polishing process of Metallographic samples.

The effect of HIUST at different pouring temperatures on modification of primary  $Mg_2Si$  can be explained by the survival of the ultrasonically induced embryos in the melt. Since these embryos

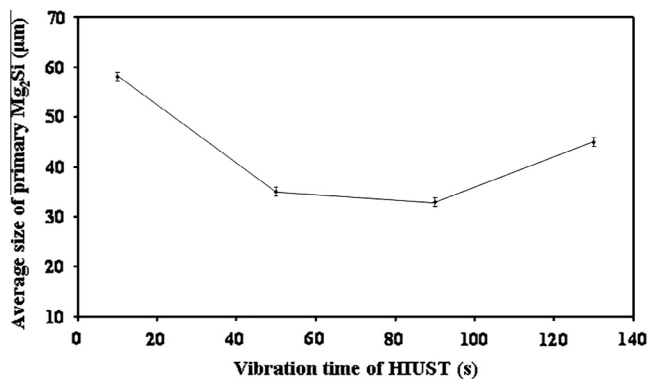


Fig. 10. Variation of average size of primary Mg<sub>2</sub>Si of the investigated hypereutectic Mg–5 wt.%Si alloys with HIUST at optimum pouring temperature of 800 °C for different vibration times.

are not thermodynamically stable (they are formed only at the interfaces of the cavitation bubble and the melt during the expansion stage of the cavitation bubbles), they will be dissolved after the cavitation bubbles are collapsed in the melt [26]. As a consequence of such instability, the number of active nuclei in the melt was quite low, as well as their thermal stability at pouring temperature (810 °C) of the investigated alloy, resulting in coarse size of primary Mg<sub>2</sub>Si, as shown in Fig. 4f. When the pouring temperature (770 °C) is closer to the liquidus temperature (767 °C) of the investigated alloy, the melt will be more viscous, so the formation of cavitation bubbles is more difficult, thus decreasing the quantity of embryos in the melt and the number of polyhedral morphology of primary Mg<sub>2</sub>Si in the final microstructure as shown in Fig. 4b. At optimum pouring temperature (800 °C in this work), the embryos life time was long enough to promote a high density of nuclei in the melt, thus leading to the development of a fine primary Mg<sub>2</sub>Si with polyhedral morphology, as shown in Fig. 4e.

The effect of HIUST at optimum pouring temperature of 800 °C for different vibration times on modification of primary Mg<sub>2</sub>Si can be explained as follows: shorter duration (10 s) of ultrasonic vibration results insufficiency nucleation in the period above the liquidus temperature of investigated alloy as well as the vibration effect by HIUST has not broken out the secondary branches and tertiary branches. Therefore, mixture of dendritic and octahedron structures of primary Mg<sub>2</sub>Si is obtained, as shown in Fig. 9a. On the other hand, the greater exothermic heating with longer duration (130 s) of ultrasonic vibration leads to increase the melt temperature in the field of ultrasonic vibration [44] so that some nuclei remelt and the average size of primary Mg<sub>2</sub>Si is coarsened as shown in Fig. 9c. So only if the optimum duration (90 s in this work) of ultrasonic vibration is applied during the solidification process of the investigated alloy, the finer polyhedral shape of primary Mg<sub>2</sub>Si can be obtained as shown in Fig. 4e.

## 5. Conclusions

- (1) The HIUST has a significant effect on the refinement and modification of primary Mg<sub>2</sub>Si in the hypereutectic Mg–5 wt.%Si alloy during the solidification process.
- (2) The modification mechanism is mainly attributed to the conjugation of two mechanisms: cavitation-enhanced heterogeneous nucleation and cavitation-induced dendrite fragmentation.
- (3) For the ultrasonic vibration time of 90 s, the coarse primary Mg<sub>2</sub>Si is obtained at both lower and higher pouring temperatures of 770 °C and 810 °C, respectively. Therefore, fine polyhedral shape of primary Mg<sub>2</sub>Si can be obtained at optimum pouring temperature of 800 °C.

- (4) At optimum pouring temperature (800 °C) of HIUST, the coarse primary Mg<sub>2</sub>Si is obtained at both lower and higher vibration times of 10 s and 130 s, respectively. Thus, fine polyhedral shape of primary Mg<sub>2</sub>Si can be obtained at optimum vibration time of 90 s.

## Acknowledgement

The authors would like to appreciate the financial support from Academy of Scientific Research and Technology in the framework of the scholarship for support of Ph.D study, Ministry of Scientific Research, Egypt.

## References

- [1] Z.Z. Shi, The crystallography of lath-shaped Mg<sub>2</sub>Sn precipitates in a Mg–Sn–Zn–Mn alloy, *J. Alloys Comp.* 559 (2013) 158–161.
- [2] L. Li, Microstructure and texture evolution during super plastic deformation of Mg–Re extruded alloy, *J. Alloys Comp.* 555 (2013) 255–262.
- [3] J.S. Zhang, Y. Sun, W.L. Cheng, Z.P. Que, Y.M. Li, L. Liushan, The effect of Ca addition on microstructures and mechanical properties of Mg–RE based alloys, *J. Alloys Comp.* 554 (2013) 110–114.
- [4] M. Cong, Z. Li, J. Liu, M. Yan, K. Chen, Y. Sun, M. Huang, C. Wang, B. Ding, S. Wang, Effect of Ca on the microstructure and tensile properties of Mg–Zn–Si alloys at ambient and elevated temperature, *J. Alloys Comp.* 539 (2012) 168–173.
- [5] Z. Huang, S. Yu, Microstructure characterization on the formation of in situ Mg<sub>2</sub>Si and MgO reinforcements in AZ91D/Flyash composites, *J. Alloys Comp.* 546 (2013) 28–40.
- [6] J. Hou, C. Li, X. Liu, Nucleating role of an effective in situ Mg<sub>3</sub>P<sub>2</sub> on Mg<sub>2</sub>Si in Mg–Al–Si alloys, *J. Alloys Comp.* 509 (2011) 735–739.
- [7] H.Y. Wang, M. Zha, B. Liu, D.M. Wang, Q.C. Jiang, Microstructural evolution behavior of Mg–5Si–1Al alloy modified with Sr–Sb during isothermal heat treatment, *J. Alloys Comp.* 480 (2009) L25–L28.
- [8] H.Y. Wang, L. Chen, B. Liu, X.R. Li, J.G. Wang, Q.C. Jiang, Heterogeneous nucleation of Mg<sub>2</sub>Si on Sr<sub>11</sub>Sb<sub>10</sub> nucleus in Mg–x(3.5, 5 wt.%) Si–1Al alloys, *Mater. Chem. Phys.* 135 (2012) 358–364.
- [9] F. Mirshahi, M. Meratian, High temperature tensile properties of modified Mg/Mg<sub>2</sub>Si in situ composite, *Mater. Des.* 33 (2012) 557–562.
- [10] X. Zhang, J. Hu, L. Ye, Y. Deng, C. Tang, L. Yang, Z. Liu, Effects of Si addition on microstructure and mechanical properties of Mg–8Gd–4Y–Nd–Zr alloy, *Mater. Des.* 43 (2013) 74–79.
- [11] J. Hu, X. Zhang, C. Tang, Y. Deng, Z. Liu, L. Yang, Microstructures and mechanical properties of the Mg–8Gd–4Y–Nd–Zn–3Si (wt%) alloy, *Mater. Sci. Eng. A* 571 (2013) 19–24.
- [12] Q.C. Jiang, H.Y. Wang, Y. Wang, B.X. Ma, J.G. Wang, Modification of Mg<sub>2</sub>Si in Mg–Si alloys with yttrium, *Mater. Sci. Eng. A* 392 (2005) 130–135.
- [13] D. Jun, K. Iwai, L.W. Fang, P.J. Hua, Effects of alternating current imposition and alkaline earth elements on modification of primary Mg<sub>2</sub>Si crystals in hypereutectic Mg–Si alloy, *Trans. Nonferrous Met. Soc. China* 19 (2009) 1051–1056.
- [14] K. Kondoh, H. Oginuma, R. Tuzuki, T. Aizawa, Magnesium matrix composite with solid-state synthesized Mg<sub>2</sub>Si dispersoids, *Mater. Trans.* 44 (2003) 611–618.
- [15] L.X. Lin, C.Y. Bin, W. Xiang, M.G. Rui, Effect of cooling rates on as-cast microstructures of Mg–9Al–xSi (x = 1, 3) alloys, *Trans. Nonferrous Met. Soc. China* 20 (2010) s393–s396.
- [16] L. Lu, K.K. Thong, M. Gupta, Mg-based composite reinforced by Mg<sub>2</sub>Si, *Compos. Sci. Technol.* 63 (2003) 627–632.
- [17] T.S. Giu, Z.J. Xue, T.C. Wen, Y.Y. Sheng, Morphology modification of Mg<sub>2</sub>Si by Sr addition in Mg–4%Si alloy, *Trans. Nonferrous Met. Soc. China* 21 (2011) 1932–1936.
- [18] R. Alizadeh, R. Mahmudi, Effects of Sb addition on the modification of Mg<sub>2</sub>Si particles and high-temperature mechanical properties of cast Mg–4Zn–2Si alloy, *J. Alloys Comp.* 509 (2011) 9195–9199.
- [19] Y. Hong, H. Yong, W.X. Gian, Influence of Sb modification on microstructures and mechanical properties of Mg<sub>2</sub>Si/AM60 composites, *Trans. Nonferrous Met. Soc. China* 20 (2010) s411–s415.
- [20] K. Chen, Z.Q. Li, J.S. Liu, J.N. Yang, Y.D. Sun, S.G. Bian, The effect of Ba addition on microstructure of in situ synthesized Mg<sub>2</sub>Si/Mg–Zn–Si composites, *J. Alloys Comp.* 487 (2009) 293–297.
- [21] N. Zheng, H.Y. Wang, Z.H. Gu, W. Wang, Q.C. Jiang, Development of an effective modifier for hypereutectic Mg–Si alloys, *J. Alloys Comp.* 463 (2008) L1–L4.
- [22] H.Y. Wang, W. Wang, M. Zha, N. Zheng, Z.H. Gu, D. Li, Q.C. Jiang, Influence of the amount of KBF<sub>4</sub> on the morphology of Mg<sub>2</sub>Si in Mg–5Si alloys, *Mater. Chem. Phys.* 108 (2008) 353–358.
- [23] E.J. Guo, B.X. Ma, L.P. Wang, Modification of Mg<sub>2</sub>Si morphology in Mg–Si alloys with Bi, *J. Mater. Process. Technol.* 206 (2008) 161–166.

- [24] Z. Na, W.H. Yuan, Z. Feng, G.Z. Hua, L. Dong, J.Q. Chuan, Modification of primary Mg<sub>2</sub>Si in Mg-5Si alloys with Y<sub>2</sub>O<sub>3</sub>, *Trans. Nonferrous Met. Soc. China* 17 (2007) s440–s443.
- [25] O.V. Abramov, *High-Intensity Ultrasonics: Theory And Industrial Applications*, First ed., Gordon and Breach Science Publishers, Amsterdam, 1998.
- [26] G.I. Eskin, *Ultrasonic Treatment of Light Alloy Melts*, First ed., Gordon and Breach Science Publishers, Amsterdam, 1998.
- [27] P.P. Bhingole, G.P. Chaudhari, Synergy of nano carbon black inoculation and high intensity ultrasonic processing in cast magnesium alloys, *Mater. Sci. Eng. A* 556 (2012) 954–961.
- [28] Z. Liang, W.G. Hua, W.S. Hua, D.W. Jiang, Effect of cooling condition on microstructure of semi-solid AZ91 slurry produced via ultrasonic vibration process, *Trans. Nonferrous Met. Soc. China* 22 (2012) 2357–2363.
- [29] M.K. Aghayani, B. Niroumand, Effects of ultrasonic treatment on microstructure and tensile strength of AZ91 magnesium alloy, *J. Alloys Comp.* 509 (2011) 114–122.
- [30] D. Gao, Z. Li, Q. Han, Q. Zhai, Effect of ultrasonic power on microstructure and mechanical properties of AZ91 alloy, *Mater. Sci. Eng. A* 502 (2009) 2–5.
- [31] X. Liu, Y. Osawa, S. Takamori, T. Mukai, Microstructure and mechanical properties of AZ91 alloy produced with ultrasonic vibration, *Mater. Sci. Eng. A* 487 (2008) 120–123.
- [32] X. Liu, Y. Osawa, S. Takamori, T. Mukai, Grain refinement of AZ91 alloy by introducing ultrasonic vibration during solidification, *Mater. Lett.* 62 (2008) 2872–2875.
- [33] Z.Z. Qiang, L.Q. Chi, C.J. Zhong, Microstructures and mechanical properties of AZ80 alloy treated by pulsed ultrasonic vibration, *Trans. Nonferrous Met. Soc. China* 18 (2008) s113–s116.
- [34] A. Ramirez, M. Qian, B. Davis, T. Wilks, D.H. StJohn, Potency of high-intensity ultrasonic treatment for grain refinement of magnesium alloys, *Scr. Mater.* 59 (2008) 19–22.
- [35] J. Lan, Y. Yang, X. Li, Microstructure and microhardness of SiC nanoparticles reinforced magnesium composites fabricated by ultrasonic method, *Mater. Sci. Eng. A* 386 (2004) 284–290.
- [36] M. E. Moussa, M. A. Waly, A. A. Nofal, A. M. El-Sheikh, Influence of ultrasonic vibration on the grain refinement and mechanical properties of AZ91 magnesium alloy, in: *Proceedings of 1st InterQuadrennial Conference in Middle East and Africa (IQCMEA-ICF): Processing, Performance and failure analysis of Engineering Materials*, Egypt 2011 pp. 103–113.
- [37] M. E. Moussa, M. A. Waly, A. A. Nofal, A. M. El-Sheikh, Effect of ultrasonic vibration and boron addition on microstructure and mechanical properties of AZ91 magnesium alloy, in: *Proceedings of 8th Arab Foundry symposium (ARABCAST 2010)*, Egypt 2010 pp. 1–14.
- [38] G.F.V. Voort, *Metallography and Microstructures*, first ed., ASM Handbook, Metals Park, OH, USA, 2004.
- [39] C. Malcolm, *Binary Alloy Phase Diagrams*, second ed., ASM International, Materials Park, OH, USA, 1996.
- [40] J.D. Hunt, K.A. Jackson, Nucleation of solid in an undercooled liquid by cavitation, *J. Appl. Phys.* 37 (1966) 254–257.
- [41] B. Patel, G.P. Chaudhari, P.P. Bhingole, Microstructural evolution in ultrasonicated AS41 magnesium alloy, *Mater. Lett.* 66 (2012) 335–338.
- [42] X. Jian, H. Xu, T.T. Meek, Q. Han, Effect of power ultrasound on solidification of aluminum A356 alloy, *Mater. Lett.* 59 (2005) 190–193.
- [43] M.C. Flemings, *Solidification Processing*, McGraw-Hill, NewYork, 1974.
- [44] L.J. Wen, T. Momono, F. Ying, J. Zheng, Effect of ultrasonic stirring on temperature distribution and grain refinement in Al–1.65%Si alloy melt, *Trans. Nonferrous Met. Soc. China* 17 (2007) 691–697.